

Journal of Materials Chemistry C

Accepted Manuscript



This is an *Accepted Manuscript*, which has been through the Royal Society of Chemistry peer review process and has been accepted for publication.

Accepted Manuscripts are published online shortly after acceptance, before technical editing, formatting and proof reading. Using this free service, authors can make their results available to the community, in citable form, before we publish the edited article. We will replace this *Accepted Manuscript* with the edited and formatted *Advance Article* as soon as it is available.

You can find more information about *Accepted Manuscripts* in the [Information for Authors](#).

Please note that technical editing may introduce minor changes to the text and/or graphics, which may alter content. The journal's standard [Terms & Conditions](#) and the [Ethical guidelines](#) still apply. In no event shall the Royal Society of Chemistry be held responsible for any errors or omissions in this *Accepted Manuscript* or any consequences arising from the use of any information it contains.

Acceptor defect participating magnetic exchange in ZnO:Cu nanocrystalline film: defect structure evolution, Cu-N synergetic role and magnetic control

Cite this: DOI: 10.1039/x0xx00000x

Received 00th January 2012,
Accepted 00th January 2012

DOI: 10.1039/x0xx00000x

www.rsc.org/

Liang Hu, Liping Zhu,* Haiping He,* Le Zhang and Zhizhen Ye

Long-term ambiguous knowledge makes individuals confused about unstable magnetic origin and some defect related issues in transition metal ions (TMs) doped ZnO system. In this paper, facile colloidal chemistry procedure is employed to prepare amine-capped ZnO:Cu nanocrystals (NCs) with optimized Cu-N defect configuration. Doping mechanism, dopant spatial distribution, valence state and defect structure are revealed in detail *via* electron microscope, electron spin resonant (ESR) and photoluminescence (PL) techniques assisted by *in-situ* chemically tracking. N-capping annealing induced acceptor defects can activate the high temperature ferromagnetism in spin-coated ZnO:Cu nanocrystalline films whereas O-capping ones cannot. Although the maximal moment of surface acceptor defects mediated ferromagnetic films ($1.58 \mu_B/\text{Cu}$) is comparable with that of bulk donor defects mediated case ($1.41 \mu_B/\text{Cu}$), the corresponding physical nature is totally distinct and the former is considered more efficient. A comparative demonstration about spin-exchange process in terms of acceptor and donor defects strongly indicates a diverse role of defects in mediating ferromagnetic ordering, like the case of carrier type-determined ferromagnetic difference. The proposal of physical (annealing) or chemical (capping) means for magnetic control in ZnO:Cu system expands the methodology of applications which utilize spin and defects as controllable states.

1 Introduction

TMs or rare-earth (RE) doped ZnO materials, as a category of theoretically predicted high Curie temperature (T_C) diluted magnetic semiconductors (DMSs), are very promising to be applied in numerous spin-based device structures.¹ Acquiring a robust ferromagnetic response independent of environmental influences is also an intermediate aim of realizing practical spintronic or magneto-optic application. Although the reports of room-temperature ferromagnetism have been numerically established, the origin of observed ferromagnetic behaviors is still the subject of ongoing research. As demonstrated in previous reports,^{2, 3} diversified magnetic phenomena are more likely caused by differences in the processing condition, which leads to different impurity and defect states including acceptor and donor ones. To pursue the underlying magnetic exchange mechanism, we have to closely monitor the evolution of defect configuration and learn more information about the interplay between impurity and defect state and the means of magnetic activation.

Subjected to much inconvenience, like the dependence on costly growth apparatus and challenging structural characterization, traditional *in-situ* investigation on doping process is actually quite tough. By the time of nanotechnology, impressive nanosized architectures and dimensional features (nanoparticle, nanorod/wire, nanoribbon, *etc.*) endow materials with more fantastic properties. Semiconductor NCs are just a great example. Based on the well-

established colloidal chemistry approaches, the delicate tuning over chemical composition and impurity distribution of the doped NCs have been possible. In general, in order to avoid impurity ejection, passivating surface states and boosting dopant-defect environment reconstruction, post-processing *via* ligand modification followed by thermal activation are quite imperative for improving original photochemical and physical properties of materials.⁴⁻⁷ To our knowledge, chemical capping has been proven an effective way to tune charge-transfer electronic structure of doped ZnO NCs, where N-capping and O-capping serve as acceptor and donor defect, respectively, which mostly depend on the dopant type.⁴ For example, only n-type capping will induce ferromagnetic appearance in ZnO:Co and otherwise will destroy ferromagnetic ordering; accordingly, p-type capping is in favor of the magnetization enhancement in ZnO:Mn and n-type not.⁸ The ligand capping as a kind of introduced surface defect can effectively mediate ferromagnetic ordering,⁹ which is different from the bulk defect mediated one. Although doped NCs have received significant concern, the distinction in ferromagnetic activation between surface and bulk defects are seldom reported. Further research in these systems from the defect structure evolution to the derived magnetic phenomena appear very essential.

For Cu-doped ZnO, the current experimental investigations progress quickly mainly due to its unique magnetic gift without the disturbance of magnetic secondary phase. Unlike magnetic TM elements of Co, Ni, and Fe, metallic copper and all of the known

copper oxide phases are non-ferromagnetic only except CuO nanoparticles.¹⁰ Even so, the dispute occurring in ZnO:Cu film and powder materials are telling a story about ambiguous diluted magnetic origin (details see Table S1). Different from the above material forms, the surface and bulk properties of free-standing NCs can be easily tailored by physical or chemical means. The early research driven by Gamelin *et al.* has offered numerous classic models to support this viewpoint occurring in oxides and non-oxides.^{8,11} But so far a systematic research idea aiming at ZnO:Cu NCs from material synthesis to structural optimization, up to correlated magnetic control has not shown up yet. Due to a specific valence-variable (*d*-state variance) and photosensitive feature of Cu element in ZnO,¹² this makes study more convenient than other doped ZnO systems, such as structure-sensitive ESR and defect-sensitive PL signal, which will better serve the exploration of structural evolution correlated ferromagnetic behaviors.

For ultra-small particles, *e.g.* NCs, if we can establish *in situ* or *ex situ* reducing doping environment, the possibility of nano-sized CuO in as-prepared NCs can be reduced to the minimum extent. And then through secondary processing, those metastable reduced copper species in ZnO host are re-oxidized into Cu²⁺ contributing to the ferromagnetism, avoiding the direct formation of CuO nanoclusters. In support of this line of thinking, we intentionally choose divalent copper (II) ions as dopant source to verify the possible reducing process in *in situ* NCs growth process. Meanwhile, among all oxidation states (Cu⁰, Cu⁺ and Cu²⁺), it is well known that the binding energy between Cu²⁺ and ZnO crystal surface is the biggest and Cu²⁺ is also more likely to be absorbed into bulk.¹³ If so, all optimized metastable oxidation states in ZnO:Cu system would not bring complexity to magnetic analysis as long as controllable preparation and careful structure characterization for samples have been done. In past years, low average atomic magnetic moment also introduced much technical difficulties to identify ferromagnetic origin and thus the advances in ZnO:Cu DMS theoretical research went on slowly to some degree. In practice, the target samples should have as big magnetic moment values as possible so as to reduce the perturbation of other magnetic sources. Recent reports have given several excellent cases to interpret the possibility of achieving a moment value close to theoretical optimum (1.73 μ_B /Cu) in ZnO:Cu system.^{2,14,15} These efforts greatly catalyze the proposal and development of some theoretical models and empirical evidences of exchange interaction between diluted spins,^{2,15,16} also trigger a very active area of DMS research. Based on the above foundations, providing insight into the relation between copper dopants and bulk/surface defects and corresponding structural evolution under different extrinsic perturbations should be a significant subject to tune magnetic structure and eventually realize magnetic control.

In this report, we first examine the issues of dopant location, valence states and possible defect configurations in N-capped ZnO:Cu colloidal NCs using electron microscope, ESR and PL techniques. Followed by spin-coating and amine activation strategy, observable evidences of acceptor mediated ferromagnetic activation are revealed. But for O-capping, there is no considerable ferromagnetic response captured in the films. The role of such kind of surface donor defects on magnetic exchange seems different from that of previously suggested bound donor defects in polycrystalline films.^{2,17} In the next analyses and discussions, we will place emphasis on the nature of these surface and bulk defects, reveal the different exchange mechanisms, and eventually realize controllable magnetization. For the sake of discussion, doped samples with variable Cu content (0.5%, 0.8%, 1.0%, 2.0%, 4.0%) are labelled as ZCO0.5, ZCO0.8, ZCO1.0, ZCO2.0 and ZCO4.0, respectively.

For control experiments, the other doping contents are also similarly denoted.

2 Experimental

2.1 Materials

Zinc acetate anhydrate (Zn(Ac)₂, 99.99%), copper (II) acetate anhydrate (Cu(Ac)₂, 99.99%), potassium hydroxide pellets (KOH, 85+%) were purchased from Sigma-Aldrich. *n*-octylamine (OA, 99+%) and glacial acetic acid (HAc, 99.8%) was purchased from Acros Organic. Other chemicals and solvents including methanol and chloroform were analytical grade reagents (Sinopharm Chemical Reagent Co.). The water (R > 18M Ω) was purified by a Milli-Q system to offer the use of preparation. All chemicals were used as received.

2.2 Synthesis of ZnO:Cu NCs

Typical dopant concentrations were set at a level below 5.0 at.% so as not to form a separate phase. Cu²⁺/Zn²⁺ molar ratio was mainly varied within 0: 100.0 (pure ZnO), 0.5: 99.5, 0.8: 99.2, 1.0: 99.0, 2.0: 98.0, 4.0: 96.0 and 100.0: 0 (pure CuO). Higher doping content was also adopted for comparison. Taking ZCO2.0 for example, first, Zn(Ac)₂ methanol solution (30 mL, 0.09 M) was loaded into a 100 mL three-necked flask and refluxed for an hour at 65°C in a water bath. Afterwards, the base solution (10 mL, 0.235 M), made from a stoichiometric amount of KOH dissolved in methanol, was added dropwise into the flask with constant stirring. After 15 min, brilliant blue Cu(Ac)₂ methanol solution (10 mL, 5.6 mM) was injected into the above precursor. And the mixture was cooled down to 50°C for dopant binding. Maintaining this temperature point (50°C), equal KOH solution (10 mL, 0.235 M) was added into reaction system again to finish the overgrowth of ZnO:Cu NCs. In this case, nominal 2.0% doped ZnO:Cu NCs were generated by stirring for another two hour and then quenched in cold water. The preparations of pure ZnO and CuO NCs were analogous to doped ones with fixed reaction temperature of 65°C. All as-prepared samples were pre-washed five times using methanol for roughly removing residual precursor ions.

2.3 Etching of ZnO:Cu NCs

Four groups of 10 μ L purified NC colloidal solution (containing 0.5 mg NCs) were diluted in 1 mL chloroform solvent, respectively. Here, acetic acid was used as etchant. Prior to the addition, a series of etchant solutions with different concentrations (3.0 \times 10⁻⁶ mM, 6.0 \times 10⁻⁶ mM, 9.0 \times 10⁻⁶ mM, and 1.2 \times 10⁻⁵ mM) with the same volume (0.5 mL) were prepared and denoted as solution A, B, C, and D, respectively. The etchant solutions were added into the NC solutions within 5 min under stirring and then the reactions were lasted for 90 min. After fully complete etching processes, all samples underwent extensive methanol and OA washing to remove the residuals from the etchant and the ions etched away from NCs. The obtained etched NC species could be further suspended in chloroform for the TEM observation and elemental analysis.

2.4 Amine bath of ZnO:Cu NCs

A given amount of pre-washed ZnO:Cu NC powders were suspended in OA reagent. Vigorous agitation and moderate heating (ca. 150°C) are needed to keep complete interaction between OA molecule and absorbed Cu ions. 2min later, the amine-treated NCs were precipitated from OA. After washed repeatedly using methanol, the resulting solids could be easily

resuspended in nonpolar solvents (*e.g.* chloroform) to form high-optical-quality colloidal solution which is more stable than untreated NCs solution. The obtained concentration of ZnO:Cu NCs in chloroform is ca. 50 mg/mL. For comparison with amine bath, a five-time washing process using methanol was conducted with other condition unchanged.

2.5 Thermal activation of nanocrystalline films

Diluted NC colloidal solutions were spin-coated onto clean 1×1 cm silicon (100) substrates with a speed of 3000 revolutions per minute (rpm). Prior to spin coating, the substrates were treated in oxygen plasma for 5 min to remove surface contamination. All treated substrates still keep diamagnetic feature. To prevent film from cracking, all films were pre-heated at 70°C until their surfaces become uniform and compact. Ten coatings could obtain a film with thickness of ca. 1.5 μm. As designed heating procedure, samples are annealed to finish amine activation in air at 400°C for 15 min on a magnetic heated stirrer (C-MAG HS 7 IKAMAG, $T_{\max} \sim 500^\circ\text{C}$). For control experiments, the same batch of films without amine capping will go through equilibrium thermal annealing treatment (900°C for 3 hrs. under N₂ atmosphere).

2.6 Characterization

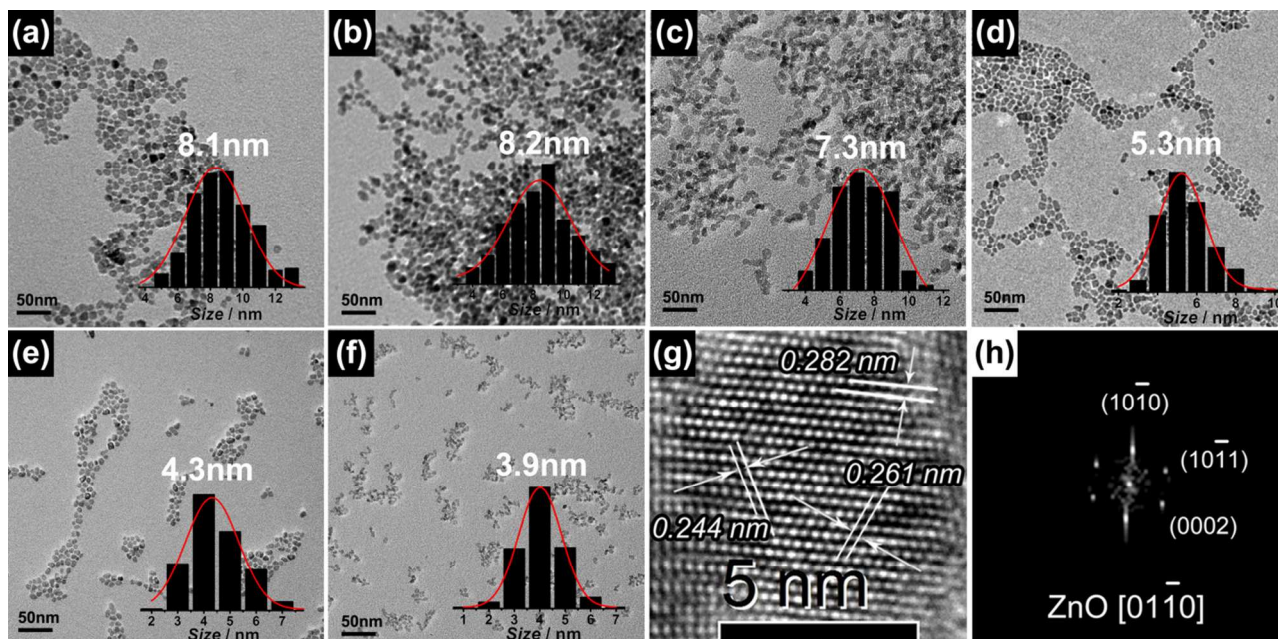


Fig. 1 Typical TEM images of N-capped ZnO:Cu NCs from the reaction of 0% (a), 0.5% (b), 0.8% (c), 1.0% (d), 2.0% (e), 4.0% (f) copper precursor, respectively. Insets in (a-f) show the corresponding size distribution histograms and average grain sizes were marked around. (g) High resolution TEM image and (h) corresponding FFT pattern of a single ZCO1.0 nanoparticle.

UV-*vis* absorption experiments were conducted on a Shimadzu UV-3600 spectrophotometer equipped with a deuterium lamp and a tungsten-halogen lamp. Fourier transform infrared (FT-IR) spectra were obtained by a Bruker Vector 22 spectrophotometer. Steady-state PL measurements were performed on an Edinburgh Instruments FLS-920 fluorescence spectrophotometer using 325 nm excitation light source from Xenon lamp. Transient decay data were recorded on the same instruments using the time-resolved mode of fluorescence spectrophotometer. X-ray photoelectron spectroscopy (XPS) was conducted in a Thermo ESCALAB 250 spectrometer using a monochromated Al K α X-ray source (1486.6 eV) in order to monitor the valence change of copper ions. All binding energy

X-ray diffraction (XRD) patterns were recorded on an X'Pert PRO system with Cu K α radiation ($\lambda = 1.5104 \text{ \AA}$) in the 2θ range from 20° to 80°. Survey transmission electron microscopy (TEM) images and selected area electron diffraction (SAED) patterns were collected using a Philips CM 200 microscope operated at 160 kV. High resolution TEM and energy dispersive X-ray spectroscopy (EDX) were conducted on a FEI TECNAI G² F20 TEM operated at 200 kV. All samples were dispersed onto ultrathin carbon-coated gold grids for element analyses. The Z-contrast scanning transmission electron microscopy (STEM) in high angle annular dark-field mode (HAADF, spatial resolution of 0.24 nm) and line-scan EDX experiments (spatial resolution of 0.144 nm) were also performed on a TECNAI G² F20 transmission electron microscope equipped with an HAADF/EDX detector. Core-loss electron energy loss spectroscopy (EELS) experiments were implemented with an energy resolution of 0.2 eV/channel and the exposure time was limited to 5 s to avoid beam damage. The obtained core-loss spectra were corrected using the zero loss peak (ZLP) position and their backgrounds were subtracted by a power-law fitting method.¹⁸ The determination of dopant concentration (including etching experiment) was carried out by inductively coupled plasma atomic emission spectrometry (ICP-AES, IRIS Intrepid IIXSP). The surface morphology of film samples were obtained by a Veeco Multimode atomic force microscopy (AFM).

data were revised by C 1s peak (284.8 eV) derived from surface hydrocarbon contamination. Temperature-dependent ESR measurements were carried out using a Bruker ESRA-300 spectrometer operating at 9.86 GHz (X-band). Magnetic hysteresis loops and temperature-variable magnetic characterization including zero-field-cooled/field-cooled (ZFC/FC) modes of samples were carried out with a superconducting quantum interference device (SQUID) magnetometer (Quantum Design MPMS2). For the ZFC case, the samples were cooled to 3 K in zero field and a fixed measuring field was then applied, followed by data acquisition at different temperature points. Likewise, for the FC data, they were directly obtained in a specified measuring field with the

system cooled to 3 K. For magnetic hysteresis loops, diamagnetic contributions from Si substrate and plastic capsule used as a sample holder have been subtracted. The magnetic force microscope (MFM) data were taken on a scanning probe microscopy (Veeco Digital Instruments) with Co/Cr-coated probe tips (top: 10-250 nm and bottom: 1-10 nm). All MFM images have been flattened with a second order of polynomial fitting.

3 Results and discussion

3.1 Spatial distribution and valence state of Cu dopants

Fig. 1(a-f) summaries the overall TEM data collected from a series of Cu-doped ZnO NCs (0~4.0%). Highly dispersed arrangement verifies a capping repulsion effect from OA molecules. Their average grain-sizes can be determined *via* a simple mathematical statistics method, which exhibits a small deviation compared with the analyses of absorption spectra (see Table 2). It is evident that increasing doping concentration leads to a decrease of NC size, which has been observed in many NC systems.¹⁹ And the doping-induced slight shape change should be ascribed to the nonequilibrium introduction of Cu dopants. High resolution TEM image and corresponding Fast Fourier Transform (FFT) pattern of a single quasi-spherical ZCO1.0 nanoparticle in Fig. 1g and 1h indicate a high degree of crystallinity of the lightly-doped sample without any observed segregations. A higher doping amount (8.0%) will induce the appearance of CuO secondary-phase (see Fig. S1) due to the solubility limit of Cu dopant in ZnO (below 1.0%).²⁰ Even so, we still obtained a fairly high doping level of at least 4.0% in such small grains. Straumal *et al.*²¹ systematically studied the doping efficiencies of different TMs into ZnO with the variation of grain size. It is revealed that a smaller grain size can significantly improve the solubility limit of dopants, well supportive of our case. Compared with most ZnO:Cu literatures (see Table S1), the doping content here is quite heavy and meets a fundamental requirement for the investigation on complex ferromagnetic behaviors.

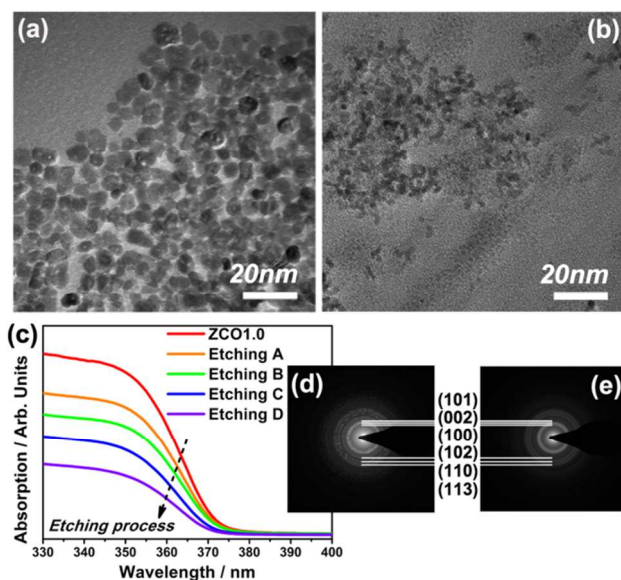


Fig. 2 A group of pictures from etching experiment. (a-b) Typical TEM images of initial and etched ZCO1.0 NCs. (c) UV-*vis* absorption spectra from the quantitative etching experiments. (d-e) SAED images from unetched and etched NCs, respectively.

According to EDX line-scan analyses (see Fig. S2), Cu is found in the whole nanoparticle. In order to confirm the distribution of Cu element in ZnO:Cu NCs, we conducted a series of chemical etching experiments aiming at ZCO1.0 NCs (TEM and UV-*vis* results see Fig. 2). As shown in Table 1, Cu dopants tend to be distributed in the core part of NCs rather than the shell part. Although a gradient doping process based on a trapped-dopant model is commonly observed in doped NCs,⁶ our results are entirely different from the previous reports of a lightly-doped core surrounded by a heavily-doped shell.^{22, 23} Wang *et al.*²⁴ also reported a similar dopant distribution in ZnO:Co NCs, where they claimed that the nonequilibrium oriented attachment in solvothermal synthesis was crucial for such an inhomogeneous doping process. As for our doping route, it is expected that some possible nonequilibrium factors are playing roles on dopant incorporation.

Table 1. Cu and Zn elemental contents corresponding to different etching stages from ICP-AES analysis of ZCO1.0 NCs.

Etching condition	Detected Cu (at.%)	Detected Zn (at.%)
Un-etched	0.89	99.11
Solution A	0.92	99.08
Solution B	1.09	98.91
Solution C	1.23	98.77
Solution D	1.53	98.47

Two groups of XRD profiles of ZnO:Cu NCs recorded before and after amine bath treatment have been shown in Fig. S3. Refinement analyses (see Table S2) reveal that all doped samples have a single-phase hexagonal wurtzite structure (JCPDS card No. 36-1451). Any Cu related secondary phases or nano-sized clusters are not found under XRD detect limit and TEM observation, indicating possible incorporation of dopant in ZnO lattice. Due to the poor contrast between Cu and Zn in XRD, the raw data could not be used to refine amounts of these ions in the wurtzite structure. However, Rietveld analysis allows the calculation of accurate cell parameters. The calculated *c*-axis lattice constants are plotted as a function of calibrated dopant content by ICP-AES in Fig. 3a. For the samples without amine bath treatment, lattice shows an expansion trend with the incorporation of smaller sized Cu²⁺ ions and finally approaches saturation at a high doping level, which implies the occurrence of nonuniform dopant adsorption on anchoring sites (not lattice sites) otherwise a contraction trend will be expected. Meanwhile, saturated expansion feature also indicates a limited adsorption capability of ZnO NC host.

The unusual lattice distortion caused by doping have been reported in several ZnO:Cu literatures and most explanations are unclear.²⁵ As for an impurity-diffusion-negligible liquid-phase synthetic strategy of doped NCs, *e.g.* low temperature reaction, the massive and nonequilibrium incorporation of dopant ions mainly depends on the trapped-dopant model. Hence, most theoretical calculations and experimental models about Cu/ZnO are suitable for the adsorption process here mainly due to some delicate discussions concerning the binding interaction between Cu species and ZnO surface.^{13, 26, 27} As theoretically given, these anchoring sites for Cu²⁺ adsorption are most likely to be vacant zinc interstitial surface sites (VZISS).^{13, 27} Bromley *et al.*¹³ based on calculation results have predicted possible charge transfer occurring between Cu species and anchoring sites, and considered the weak "reducing agent" providing electrons as an undefined deep-level trap on the surface or in the bulk of ZnO. Yoshihara *et al.*²⁶ further proposed Cu was bonded more weakly to the Zn face than O face. Meanwhile, this kind of bonding is also accompanied with some charge transfer processes. But for the decisive charge donors, they both have not fully explored them as yet. In the Section 3.2 and 3.3, we will discuss this kind of chemisorption in detail and preliminarily give the essence of binding interaction.

When additional amine bath is employed, ZnO:Cu NCs exhibit a reversed lattice distortion with dopant increase, indicating the

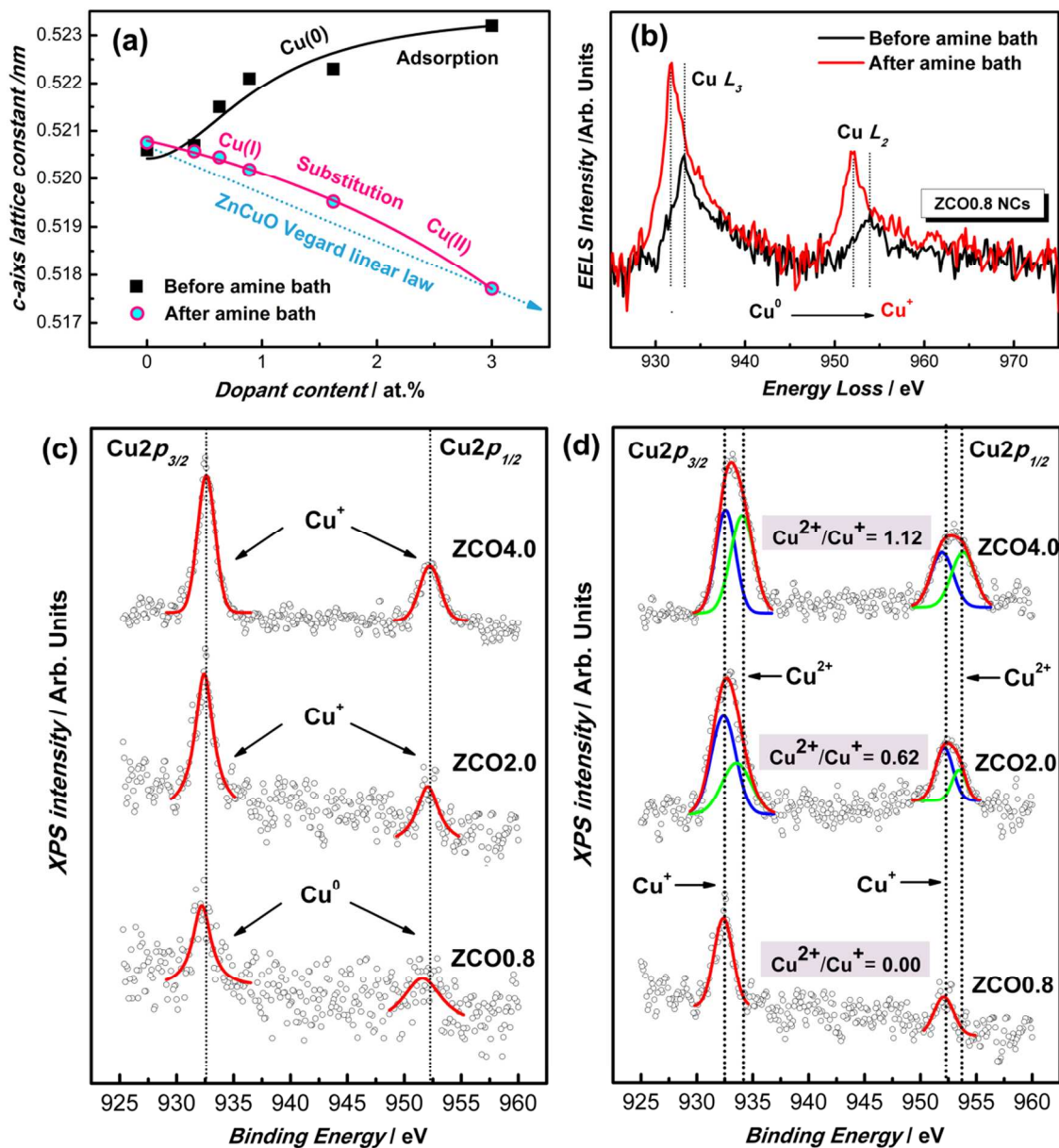


Fig. 3 (a) The dependence of *c*-axis lattice constant with incorporated Cu content. (b) Typical core-loss EELS comparison of Cu $L_{2,3}$ in ZCO0.8 NCs before and after amine treatment. (c-d) Cu 2*p* core-level XPS spectra of ZnO:Cu NCs with variable doping content (0.8%, 2.0% and 4.0%) before (a) and after (b) amine bath treatment. Standard Cu 2*p*_{3/2} and 2*p*_{1/2} positions of Cu⁺ and Cu²⁺ are marked as references.

possible structural transformation. Since increased Cu concentration induces a contractive lattice, the incorporation of Cu²⁺ into substitutional sites in lattice can be expected as the radius of Cu²⁺ (0.057 nm) is smaller than that of Zn²⁺ (0.06 nm).²⁸ Moreover, there is a discrepancy between ZnCuO alloying related Vegard's law and actual strain curve. Combined with the XPS analysis in Fig. 3d, after amine bath treatment, Cu species are mainly in the form of divalence and monovalence. Hence, we reasonably attribute this discrepancy to the disturbance of bigger sized Cu⁺ ions. Back to amine-bath-untreated samples, all Cu 2*p* core-level XPS spectra in Fig. 3c point to the nature of reduced Cu ions (Cu^{0/+}). Due to the limitation of XPS in distinguishing between Cu⁰ and Cu⁺ ions, further valence confirmation can be done by micro-zone EELS technique aiming at an isolated ZCO0.8 nanoparticle. By comparing the measured shape and intensity of Cu $L_{2,3}$ edges of ZnO:Cu NCs with standard samples

including Cu, Cu₂O and CuO (see Fig. S4), the identification for two sets of profiles in Fig. 3b should be different. The measured EELS peaks in amine-bath-untreated sample are very broad and asymmetric. It is a typical footprint of neutral Cu species. According to a full-spectrum UV-vis absorption analysis (see Fig. S5), exponent-like absorption characteristics rather than surface plasma resonance (SPR) absorption in visible range reveals a sort of continuously band-like energy-level structure, suggestive of the presence of atomic-level neutral Cu rather than nanosized metallic Cu clusters. Not all Cu species can be reduced to neutral states. Like what we observed in Fig. S6, more involved Cu²⁺ can be only partially reduced to Cu⁺, which also indirectly reflects a limited reduction capability of ZnO NCs.

On the contrary, the EELS peaks of amine-bath-treated sample are relatively sharp and symmetric, similar with that of

Cu₂O and CuO, indicating the hybridized state of 3d and 4p orbitals.²⁹ Considering peak width and chemical shift more close to that of Cu₂O, the majority of Cu element in amine-bath-treated NCs are monovalent. In addition, as more Cu dopants are added, Cu⁺ and Cu²⁺ mixed XPS spectra gradually appear and a higher doping level corresponds to a larger Cu²⁺ portion (see Fig. 3d). It can be speculated that, based on the N-capping mediated structural reconstruction and charge transfer, which are driven by amine bath treatment, such a transformation of spatial distribution and valence state of Cu dopants is feasible, *i.e.* from neutral/ monovalent Cu in VZISS to substitutional monovalent/divalent Cu ions. The disappearance of exponent-like visible absorption feature after amine bath (see Fig. S5) can well explain the above in-diffusion behavior of neutral/ monovalent Cu species. Cheng *et al.*³⁰ observed a similar coordination change in ZnO:Mn NCs *via* N- or S-capping, where they claimed an improved Mn solubility in ZnO NCs is due to Mn-N or Mn-S orbital hybridization. Likewise, Cu solubility in our samples is also promoted by amine capping, which is based on the change of dopant

incorporation model from saturated adsorption to Vegard's law-like substitution doping. Even so, one-pot amine bath does not induce the appearance of room temperature ferromagnetism (see Fig. S12), which is possibly correlated with the dominance of diamagnetic Cu⁺ ions with *d*¹⁰ electronic configuration.

3.2 Bandgap modification and Cu-N bonding of doped NCs

If divalent copper ions are successfully involved into ZnO lattice, bandgap modification will be expected. Recent theoretical study based on density functional theory has revealed a bandgap reduction with Cu substitutionally doped into ZnO due to the strong *p-d* mixing of Cu and O in ZnO:Cu.³¹ As to amine-bath-treated NCs, the UV-*vis* absorption spectra of different samples are shown in Fig. S5 and their optical bandgap (E_g) values are calculated by a sigmoidal function fitting.³² We apply these E_g values in effective mass model³³ to estimate mean grain sizes and the results are plotted in Table 2.

Table 2. The summary of element analysis, size distribution and magnetic property from ZnO:Cu granular films.

Cu content in precursors (at.%)	Cu content in NCs (at.%)	Optically determined grain size (nm)	Statistic grain size (nm)	Mean Cu number (/NC)	M_s (μ_B /Cu) ^a	M_s (μ_B /Cu) ^b
0	0	7.5	8.1	0	-	-
0.5	0.41	6.8	8.2	50	1.40	0.39
0.8	0.63	6.4	7.3	54	1.25	1.03
1.0	0.89	5.8	5.3	29	1.18	1.41
2.0	1.62	5.5	4.3	28	0.34	0.33
4.0	3.00	5.3	3.9	39	0.04	0.13

^a Amine-activated ferromagnetic films; ^b Dual-donor-activated ferromagnetic films

Theoretically, due to a joint effect of *p-d* hybridization and quantum size factor, the optically-determined size will deviate from the observed real size by TEM. Through a calibrated standard Brus curve using pure ZnO NCs, the E_g derivation only from *p-d* hybridization contribution rather than quantum size effect can be directly observed in Fig. 4, which is considered as the difference between the standard Brus curve value and the measured value. Here, the *p-d* hybridization contribution shows a nonmonotonic dependence on Cu concentration. In other words, it is negative initially, passes through an inflection at 0.8~1.0% of Cu content, and then positive with increased Cu concentration. We can well understand the positive *p-d* hybridization due to the contribution of substitutional copper ions over zinc sites.³¹ For the negative one, R. B. Bylsma *et al.*³⁴ and R. Viswanatha *et al.*³⁵ also observed similar phenomenon in Cu or Mn doped ZnO and even Mn-doped ZnSe system, where they claim that this abnormality is strongly connected with bandgap bowing in a short-ranged and disordered spin system by means of spin exchange interaction between *d* electrons of TMs and the *s* and *p* carriers of the host bands. Interestingly, such an abnormal phenomenon just corresponds to the variation trend of Cu valence state from +1 to +2 with increased Cu content. Therefore, this unique dependence of bandgap on Cu content also reflects the occurrence of Cu substitution transformation *via* amine bath treatment.

Q. Ma *et al.*³⁶ experimentally suggested Cu substitution may not be the only factor for the occurrence of ferromagnetism and the increased covalence of Cu_{Zn}-O bond should be more necessary for Cu spin alignment. FT-IR spectrum is a sensitive characterization tool, which can help individuals quickly grasp the bonding feature in doped systems. From Fig. 5a, the stretching mode of ZnO NCs can be detected at the band of 478 cm⁻¹, which corresponds to the vibration of Zn-O.³⁷ For comparison, we also prepared CuO NCs, in

which Cu-O stretching vibration is located at 474, 515 and 717 cm⁻¹.

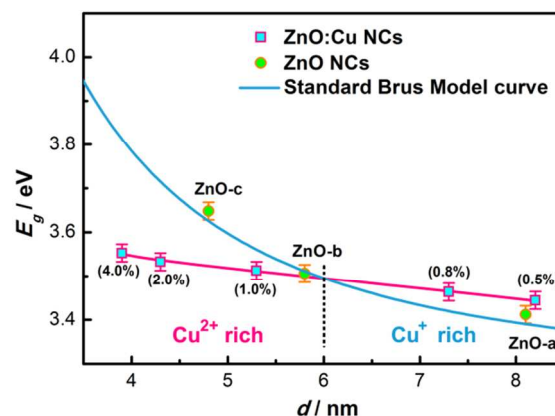


Fig. 4 Extracted optical E_g values vs. grain size (d). The undoped samples of ZnO-a ($d \sim 8.2$ nm), ZnO-b ($d \sim 5.8$ nm), and ZnO-c ($d \sim 4.8$ nm) were plotted for calibrating standard Brus Model curve.

absence of Cu-O from CuO in doped ZnO also excludes the presence of CuO secondary phase. The peaks between 3300-3500 cm⁻¹ and at 717 and 1607 cm⁻¹ are ascribed to N-H stretching and deformation vibrations, respectively,³⁹ demonstrating a robust binding of OA molecules to ZnO surface. In addition to the above, a continuous red-shift of 13 cm⁻¹ towards a lower wavenumber direction of Zn-O vibration can be observed from pure ZnO to ZCO4.0 NCs in Fig. 5b. Using a two-atom interaction model, the vibrational frequency of a peak (defined as ν) is a function of the bond force constant (defined as k) and reduced mass (defined as μ).⁴⁰

$$\nu = 1/2\pi c \sqrt{k/\mu} \quad (1)$$

with c being the speed of light and μ being related to the atomic mass of each atom, that is

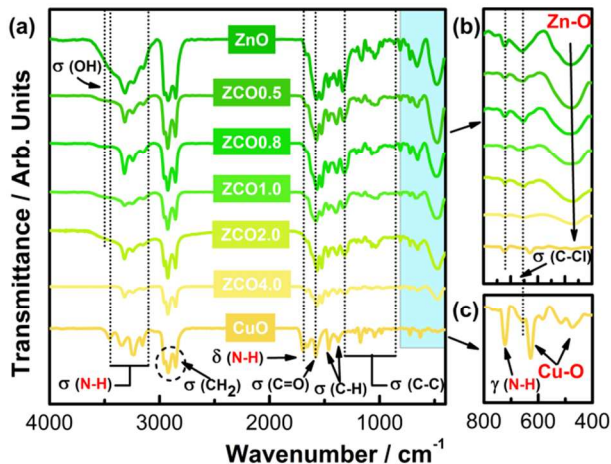


Fig. 5 FT-IR spectra of amine-capped Cu-doped ZnO NCs with different Cu/Zn molar ratios. (a) Survey scans of all samples. (b-c) Partial enlarged spectra at low frequency absorption bands (400–800 cm^{-1})

$$\mu = \frac{M_{TM} \times M_O}{M_{TM} + M_O} \quad (2)$$

According to further reduction, we could obtain

$$\nu \cong 130.2 \sqrt{k/\mu} \text{ cm}^{-1} \quad (3)$$

Due to similar reduced mass, the red-shift of IR peak in NCs should be attributed to the decrease of bond force constant k , which is closely related with the increased covalence of Zn-O replaced by Cu-N. On the other hand, the peak intensity of Zn-O vibration appears a declining tendency as Cu content grows, revealing the disruption of lattice integrity and structural disorder.⁴¹ Taking all of factors together, it is believed that the doping-induced spectral change strongly coincides with the fact of the incorporation of Cu-N into ZnO lattice. It is worth noting that, the broad structureless absorption at 3650 cm^{-1} , corresponding to O-H stretching vibration, is largely suppressed in doped samples except in pure ZnO NCs. In essence, this vibration is donor-like.⁸ With the incorporation of Cu^{2+} , the charge transfer between donors and Cu acceptors will happen and gives rise to the weakening of O-H stretching vibration. When OA-capped nanocrystalline films are heated at 400°C , there are no more amine ligand fragments left in the surface and bulk of ZnO:Cu (see Fig. S7 and Fig. S8) and thus they can be further characterized as completely inorganics with a slightly hydroxylated surface and a deeply diffused N impurity distribution.

3.3 Dopant incorporation and coordination transformation

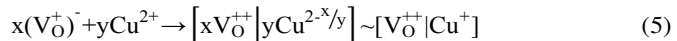
It is generally believed that doping efficiency is directly related to the adsorption ability of ions on the surface.⁴² This adsorption effect might be fairly large, *e.g.* about half of the Co^{2+} used for the synthesis of ZnO:Co NCs are adsorbed at the NCs' surface;⁴³ and even we could see the absolute binding of dopants to the surface of CdS NCs.⁴⁴ The surface of ZnO NCs in our preparation is negative potential (ζ -potential: -26 mV) due to the residual negatively charged ions, *e.g.* hydroxyl and acetate ions, and thus their presence makes the adsorption of Cu^{2+} on the anion sites possible. Due to ionic nonstoichiometry

in ZnO NCs, donor defects, *e.g.* oxygen vacancy (V_O) and interstitial zinc (Zn_i), will delocalize their bound electrons to the neighbouring Cu species (especially high oxidation state Cu^{2+}), leading to the reduction of Cu^{2+} to Cu^+ .² In this process, the thermodynamic drive force can be expressed as follows.

$$\Delta G_{\text{Red}} = eE(\text{ZnO}^+/\text{ZnO}) - eE(\text{Cu}^{2+}/\text{Cu}^+) - e^2/4\pi\epsilon\epsilon_0 R \quad (4)$$

where R is the donor-acceptor pair (DAP) distance, ϵ_0 is the vacuum permittivity, and ϵ is the static dielectric constant of bulk ZnO; $E(\text{Cu}^{2+}/\text{Cu}^+)$ is the redox potential of $\text{Cu}^{2+}/\text{Cu}^+$ redox couple in methanol ($+0.21 \text{ V}$ vs. SCE) and $E(\text{ZnO}^+/\text{ZnO})$ is the redox potential of the electron on the highest occupied energy level of the semiconductor particle.⁴⁵

The energy-level position of singly-ionized V_O (V_O^+) in ZnO:Cu nano-granular film has been deduced in our previous work according to DAP model.² It is found to be about 0.87 eV below the conduction band minimum (CBM), comparable with 0.9 eV observed in bulk ZnO.⁴⁶ At normal condition, this V_O level cannot transfer electrons to the CBM thermally and hence 0.87 eV is considered as an upper limit of oxidation potential. Since the redox potential of the CBM of ZnO NCs is -0.8 V vs. SCE,⁴⁷ the redox potential of the electrons bound to V_O in ZnO NCs is $+0.07 \text{ V}$ vs. SCE, namely $-0.8+0.87 \text{ V}$. This value ($+0.07 \text{ V}$) is smaller than $E(\text{Cu}^{2+}/\text{Cu}^+)$ ($+0.21 \text{ V}$ vs. SCE) and thus the thermodynamic reduction of Cu^{2+} to Cu^+ is allowed. If so, adsorbed Cu^{2+} ions can interplay with V_O^+ defects on the surface of the NCs, leading to the following charge-transfer process.



Here, the ratio of x/y measures the reduction ability of V_O for Cu^{2+} . Based on a hybrid QM/MM embedding model,¹³ in general, the transferred charge can be estimated to be between 0.5 and 1 e , which means a V_O^+ defect can share electrons with at most two Cu^{2+} ions simultaneously. Hence, under heavy doping condition, incomplete reduced Cu^+ ions are dominant. For $x=2y$, that is, two V_O^+ defects transfer electrons to Cu^{2+} , which is often the case of diluted or light doping, Cu^{2+} can be totally reduced to neutral state.

If so, from the kinetic perspective, the growth of ZnO:Cu NCs must be controlled essentially by two processes. One is the diffusion process of the reactants to the surface of the growing NCs and the second one is the reaction at the surface of the NCs to incorporate the dopant as a part of the growth process. In order to capture every intermediate growth stage, we choose the slowly-grown ZCO4.0 NCs to reveal the possible growth models. Meanwhile, the growth of pure ZnO NCs was monitored for control experiments. As shown in Fig. 6a, pure ZnO NCs follow a linear growth curve ($d^3 \sim t$), while for the doped sample, in the early reaction stage, there exists a deviation under the same reaction condition. This slow reaction-limited growth process should be closely linked with the chemical adsorption of Cu dopants. We assume that doping is controlled by diffusion and reaction rate. Through fitting the experimental results obtained by time-dependent absorption spectra to the formula ($t = Bd^3 + Cd^2 + D$) in Fig. 6b,⁴⁸ we find a well-matched relationship between experiment and theory, further confirming our prediction of surface chemisorption under the participation of V_O^+ defect species.

Although X-ray fine absorption spectra appear more convincing in confirming impurity local structure, the similar atomic mass between Cu and Zn element and a low doping level make direct access to structural information in ZnO:Cu NCs fairly inconvenient. The use of ESR technique offers some advantages over the generally used EXAFS setup. It owns a higher sensitivity for the study of lightly doped DMS samples

and its resonant character allows one to easily discriminate different paramagnetic species in a specific ligand field, which will help us to speculate some possible structural configurations more quickly. It is well-known that Cu^{2+} with electronic spin $S = 1/2$ and nuclear spin $I = 3/2$ will give rise to an ESR signal

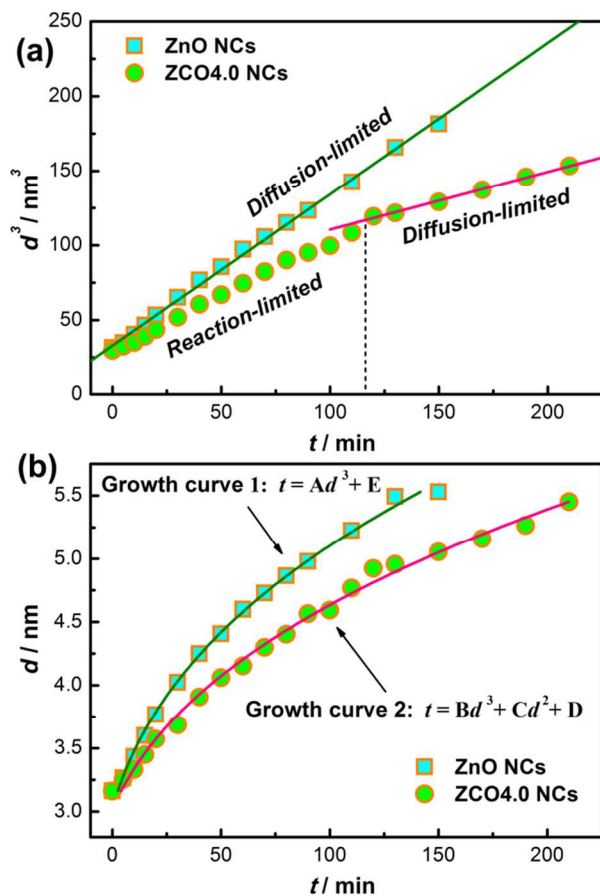


Fig. 6 (a) The cube of mean grain size (d) of ZnO and ZCO4.0 NCs without amine bath shown as a function of reaction time (t). (b) The optimized fits of growth curves from ZnO and ZCO4.0 NCs without amine bath using the forms of $t = Ad^3 + E$ and $t = Bd^3 + Cd^2 + D$, respectively. The corresponding values of parameter A , B , C , D and E are 1.0, 1.4, 0.6, -52.0 and -32.9.

with four-line hyperfine structure.⁴⁹ Fig. 7a shows a series of ESR spectra recorded from different processed ZCO0.8 NC samples. For the case of only Cu adsorption on ZnO surface, the narrow linewidth and the presence of axis symmetric signals clearly demonstrate that the Cu^{2+} species are most probably bound to the outer vacancy structure.^{49, 50} Hyperfine splitting ($g_{xx} = g_{yy} = g_{\perp} \sim 2.08$, $g_{zz} = g_{\parallel} = g_{\parallel} \sim 2.41$, $A_{\parallel} = 13.5$ mT) also reflects highly-dispersive Cu species distribution.⁵¹ Different from simple adsorption or ion exchange of Cu^{2+} ions with other solids (e.g. zeolites and clay minerals) leading to the lossless ESR signal, the widened ESR spectrum in Fig. 7a compared with free Cu^{2+} ions (see Fig. S9) indicates a decrease of the relaxation time of Cu^{2+} upon adsorption onto the NCs' surface.⁴⁵ Due to a limited surface defect density in pure well-grown ZnO NCs, only a portion of Cu^{2+} ions are reduced to neutral Cu. Cu^{2+} related resonant peaks still remain in a large part.

Punnoose *et al.* and Leofanti *et al.* both have observed similar signals with $g_{\perp} \sim 2.05$, $g_{\parallel} \sim 2.3$ and $A_{\parallel} = 15$ mT.^{49, 50} They argued that Cu^{2+} located at octahedral vacancies provided by alumina surface should be responsible for this hyperfine splitting. Since octahedral interstitial voids in ZnO have been computed to be 0.9 eV more stable than tetrahedral ones for Cu atom,⁵² the lattice relaxation of

Cu atoms in VZISS is very small, leading to Cu–O bond length of 1.89–2.07 Å.^{13, 53} That is to say, the first nearest neighbors surrounding Cu species are three oxygen ions not belonging to the zinc sublattice. The presence of V_{O} defects directly establishes a bridge between interstitial Cu (Cu_i) and charge traps and helps better

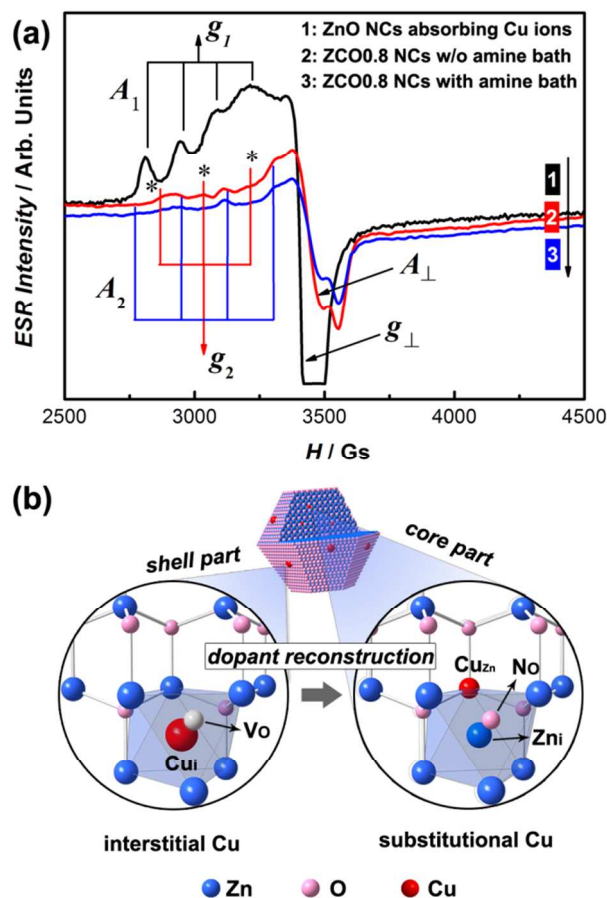


Fig. 7 (a) ESR spectral comparison at room temperature for the case of Cu ions adsorption on ZnO NCs, as-prepared ZCO0.8 NCs, and amine-bath-treated ZCO0.8 NCs. (b) The illustrative configuration of dopant-defect complex in Cu-doped ZnO NCs.

finish charge transfer. According to $\text{ZnO}:\text{Cu}_i$ model proposed by A. Hausmann *et al.*,⁵⁴ Cu atoms located at interstitial sites (Cu_{Zn_6}) will undergo a weak dynamic Jahn-Teller effect and have an electron configuration $3d^9 4s^1 4p^2$. Splitting energy-level of ${}^6P_{3/2}$ has an experimental g_{\parallel} value of 2.4 ± 0.1 , which coincides with our case and reveals a highly-reduced Cu dopant. The possible dopant-defect configuration is shown in the left part of Fig. 6b.

In order to obtain more information about bulk doping, we compared a pair of ESR signals of ZCO0.8 NCs before and after amine bath treatment. For amine-bath-untreated ZCO0.8 NCs, a set of new peaks (three-line, denoted as * in Fig. 7a) are superimposed on original four-line structure of with decreased intensity and hyperfine coupling constant ($A_2 = 9$ mT). Appearance of the A_{\perp} components shows that the concentration of the Cu^{2+} species is extremely low (beyond XPS and EELS detection limit). Most of Cu^{2+} ions have been reduced and thus almost cause the full elimination of the spin-spin interaction. For $g_2 \sim 2.36$ located at the centre of the participated seven-line g_{\parallel} , this position is very similar with the case of mix-valence (+1/+2) Cu ions complex.⁵⁵ As a rule, if an unpaired electron is trapped on one Cu ion ($I = 3/2$), a four-line ESR spectrum will be observed; conversely, seven-line spectrum

indicates that unpaired electron will hop between two identical Cu ions.⁵⁶ After amine bath treatment, additional three-line disappears, revealing a potential electron delocalization effect from Cu species.

So, how do we understand this transformation process? For the low surface coverage (below 33%) of Cu on ZnO, Cu ions are weakly cationic and practically clustered into planar islands rather than polyhedral islands with a partial positive charge by the interaction with ZnO surface.^{13, 26} Among all the Cu species, higher oxidation states will result in larger binding energy with ZnO surface.¹³ Neutral copper is positioned highest in the VZISS and is most weakly bound to the surface. Meanwhile, the lowest lying Cu^{2+} shows a tendency to adsorb relatively deeply into the surface and would be the most likely species to be adsorbed into the bulk due to the smallest ionic radii.¹³ Through a thermally-mediated amine bath process, on one hand, the N atoms in OA molecules diffuse into V_O sites and its weak electronegativity compared with V_O determines a reverse charge transfer process between adsorbed neutral/ monovalent Cu species and N atoms on O sites (N_O). Hence, a higher oxidation state (Cu^{+2+}) can be favorably formed. On the other hand, due to Cu-N bonding effect, oxidized Cu species have a tendency to occupy Zn sites with N atoms diffusion.⁵⁷ Here, we highly emphasize an unusual doping strategy. In other words,

the first is to pin dopants by intrinsic defect (V_O) in nonequilibrium and then to dissolve them into lattice by co-doping agent (N-capping). Under the guidance of this idea, dopant solubility can be largely improved without resulting in metal nanoclusters, showing an advantage over other preparation routes. For example, the early experiment *via* solvothermal method would produce ZnO:Cu NCs including metallic Cu clusters.²³ The similar reduction trend happens frequently especially using some nonequilibrium doping strategy such as pulsed laser deposition (PLD) and molecule beam epitaxy (MBE).⁵⁸ French *et al.*²⁷ discussed a dynamical equilibrium between planar and polyhedral Cu clusters and they concluded that the adsorption ability of anchor sites is the key factor for stabilizing copper clusters with different morphologies, by which the growth of metal clusters can be controlled. For our study, based on a moderate anchoring capability, which can be tuned by surface chemical potential and V_O density, atomic-level planar Cu cluster will in-diffuse into substitution sites rather than secondarily grow up in terms of segregated metal Cu or planar CuO phase.^{10, 23} Because of the incomplete N diffusion in amine bath, further optimizations of defect structure and the proportion between Cu^+ and Cu^{2+} with the aid of N-capping annealing are essential.

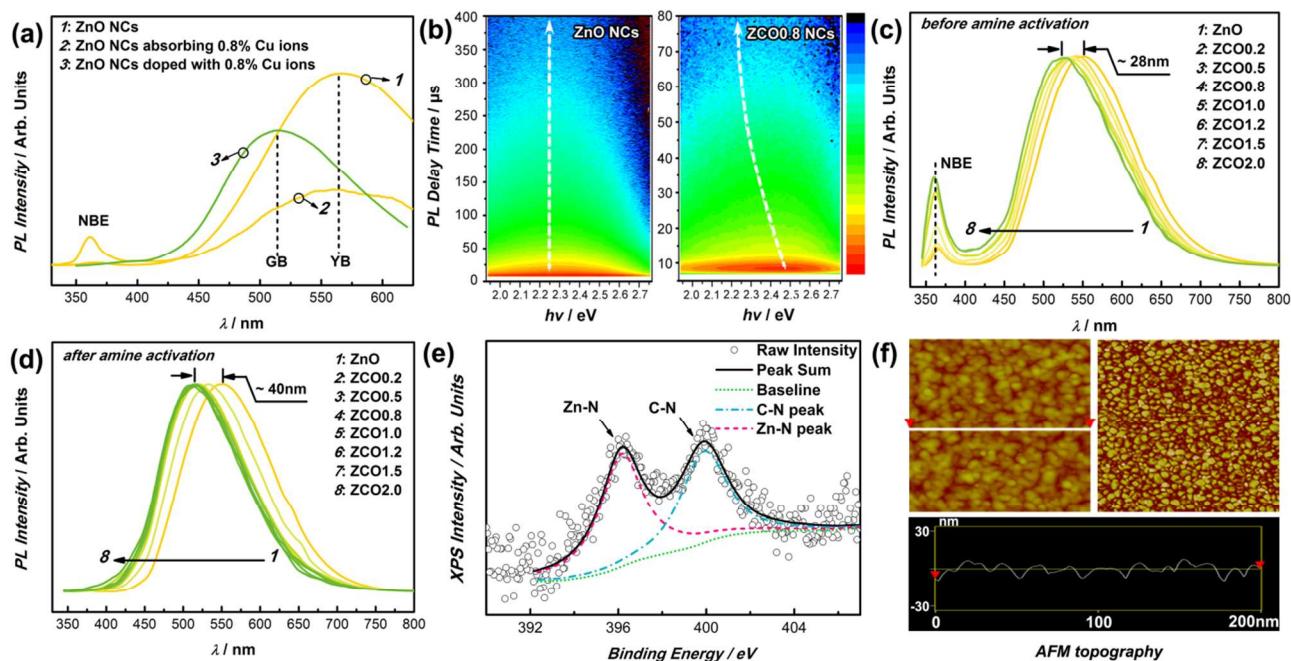


Fig. 8 (a) Room-temperature PL spectra of ZnO NCs before and after adsorption of Cu^{2+} ions. The PL signal from amine-capped ZCO0.8 NCs is shown here for comparison. (b) Time-resolved PL spectra derived from amine-capped ZnO and ZCO0.8 NCs. (c-d) Dopant content dependent PL spectral evolution for spin-coated granular films (c) before and (d) after amine annealing activation. All emissions were excited at $\lambda = 325$ nm and their peaks were normalized for the observation of a shift from YB to GB. (e) XPS spectra and fitted peaks of N 1s for amine-annealed ZCO0.8 film. (f) A pair of AFM height and phase images from amine-annealed ZCO0.8 film (200×200 nm). Line-scan topology shows a compact packing of pseudospherical particles.

3.4 Amine activation and PL evolution

Unlike Cu species in VZISS, neutral Cu substitution over zinc sites (Cu_Zn) will generate ground state g -factors of $g_{\parallel} = 0.73$ and $g_{\perp} = 1.48$, and a crystal field splitting energy 5700–5800 cm^{-1} within IR region can be observed at liquid helium temperature.^{59, 60} Since N diffusion in ZnO lowers original spatial symmetry and induces Jahn-Teller distortion, the interplay of spin-orbit and Jahn-Teller may lead to a double well potential for Cu atoms and one of them can be metastable.⁶¹ Hence, the Cu atoms in the metastable state will own an extremely long relaxation time and lead to the quenching of Cu^{2+}

g -factor. $\text{Cu} (^2T_2)$ splitting will be also un-observable. Even so, Cu^{2+} related light emission still remains. By steady state PL measurements, the status of Cu dopants located at substitutional sites can be further confirmed.

First, Fig. 8a presents the typical PL spectra for pure ZnO NCs before and after Cu adsorption at room temperature. The as-prepared ZnO NCs exhibit a remarkable yellow band (YB) emission peak at 560 nm with the absence of near band edge (NBE) emission. The character of visible emission is often supported by the fact that many point defects (V_O , V_Zn , O_i , Zn_i , *etc.*) or surface states are present in the NCs.⁶² In order to confirm the origin of YB emission, 0.8% Cu

ions are employed to study the effect of adsorbed Cu species on ZnO. Considering the diffusion barrier in NCs is larger than that in bulk, even if the native defects are present, dopant atoms cannot gain sufficient energy to diffuse into the body of NCs, especially at low synthetic temperature.⁶ So, the diffusion process of adsorbed Cu ions becomes negligible. Experiment results indicate YB is largely suppressed with enhanced NBE emission. In this process, we also monitored the variation of ESR spectra. With the incorporation of Cu^{2+} , the paramagnetic signal (g -value of *ca.* 2.0) of V_O^+ disappeared,² corresponding to the decrease of YB emission. As mentioned above, in this process, only V_O^+ participated in charge transfer with Cu ions. Therefore, the dismissed YB emission should be closely linked with V_O^+ defect. It is known that the trapping of electrons on ZnO surface is an extremely fast process and is completed within 18 ps.⁶³ Normally, photo-generated holes can almost simultaneously tunnel to V_O^+ and YB emission is generated.^{62, 64} Except for V_O^+ , surface-bonded hydroxides and adsorbed oxygen species capable of scavenging the photogenerated carriers may be also responsible for this YB emission.⁶⁴ When the sample is vacuum-treated and dried (see Fig. S10), the broad YB emission still exists, ruling out a dominant origin from adsorbed oxygen or hydroxyl species. Here, we assigned V_O^+ as the main origin of YB emission accordingly.

Since the charge transfer from ZnO to Cu^{2+} ions is also pretty fast (*ca.* 32 ps),⁶⁵ the captured photoelectrons in V_O^+ have not enough localization time to wait the recombination with

photogenerated holes and are immediately transferred to Cu^{2+} . The recombination path responsible for YB emission is thus blocked. The passivation of surface states opens up NBE radiant recombination route. In other words, the adsorbed Cu species in terms of planar Cu clusters take a modification effect on ZnO NC surface. As opposed to undoped NCs, doped NCs in Fig. 8a exhibit a red-shift emission feature with peak at *ca.* 500nm (GB). Here, it can be understood that incorporated Cu ions in lattice introduce deep-acceptor centers (*i.e.* Cu_Zn) and contribute to the popular Cu-related GB emission.^{60, 66} Specifically, Cu atoms will diffuse into Zn sites and push Zn atoms from lattice sites into interstitial sites (Zn_i). A dopant-defect complex $\text{Zn}_\text{i}^+\text{Cu}^+$ can be formed.² The transferred hole from the d -shell of Cu atom occupies a neighboring orbital perturbed by Zn_i and obtained $\text{Zn}_\text{i}^+\text{Cu}^+$ can be treated as intermediately-formed excited state (Cu^+, h). The transfer of delocalized hole to d -shell electron induces the occurrence of Cu related GB emission. Related defect complex configuration has been shown in the right panel of Fig. 5b. Time-resolved PL is conducted to observe possible radiant recombination channels. According to Fig. 8b, GB peak shifts to the YB area with delay time. Since YB has a longer lifetime, its relative contribution to the overall emission increases with increasing time. Finally, the spectrum recorded at very long time closely matches the steady-state emission spectrum of pure ZnO. This fact clearly reveals the presence of two groups of recombination channels, that is, Cu doping induced GB transition and V_O induced intrinsic YB transition.

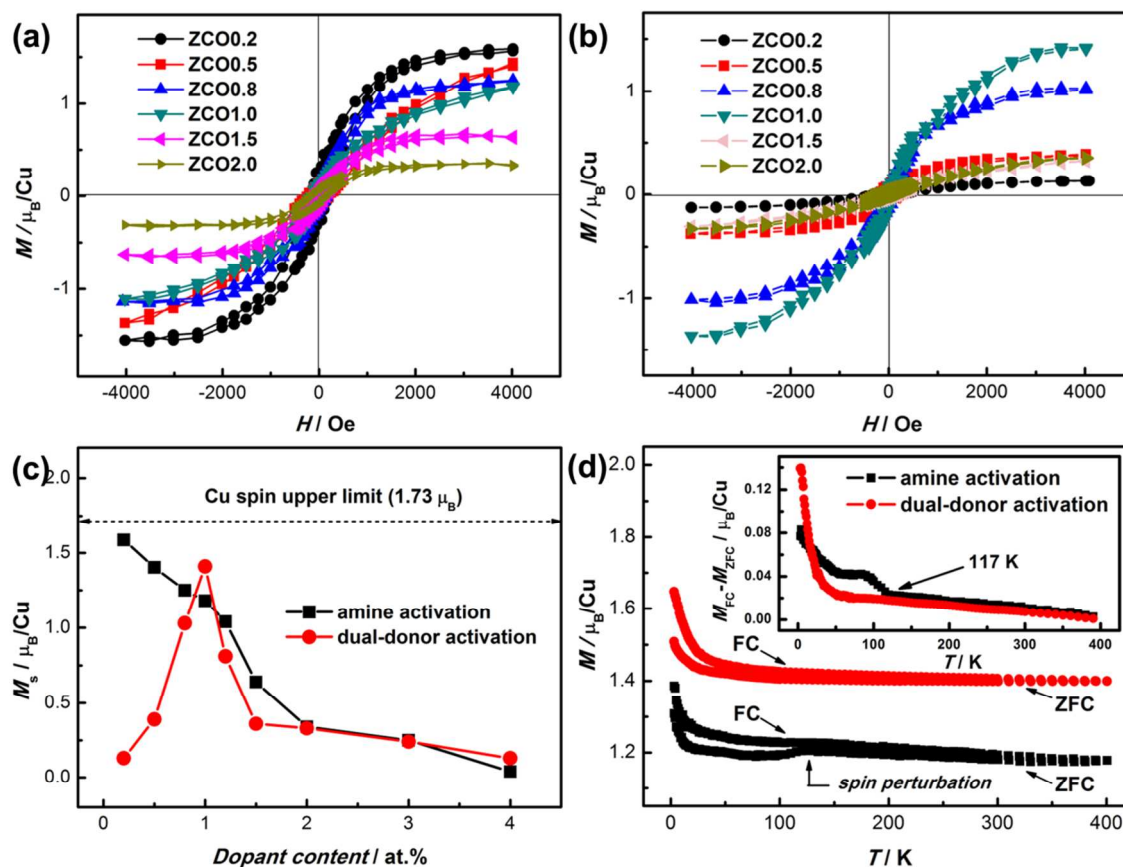


Fig. 9 A series of magnetic hysteresis loops of (a) amine-activated and (b) dual-donor-activated ZnO:Cu ferromagnetic films. (c) The dependence of M_s on dopant content with the involvement of d^0 -ferromagnetism compensation and AFM coupling. (d) The comparison of ZFC and FC curves for two types of ZCO1.0 ferromagnetic films at a fixed field (2000 Oe). In the inset, the difference of moment between FC and ZFC curve is also plotted against temperature.

It is noteworthy that, the luminescent behavior of amine-activated NC films with doping concentration is entirely different from inactivated ones. From Fig. 8c and 8d, amine activation makes

the continuous shift of defect peak larger (28 nm to 40 nm) and NBE emission quenched. This can be understood qualitatively by a fact that Cu species in VZISS are diffusing into substitutional sites with

the assistance of N atoms and the latter come from surface capped ligand molecules containing N element.⁴ Several theoretical and experimental results have supported the possibility of Cu-N co-doping into ZnO lattice and proven a potential $\text{Cu}_{\text{Zn}}\text{-N-Cu}_{\text{Zn}}$ spin exchange mechanism.⁶⁷ Like Mn-doped ZnO,⁴ such a similar structural configuration possibly determines a more robust acceptor impurity pinning environment, directly contributing to more intensive GB emission. To verify the formation of Cu-N bonds, we chose typical amine-annealed ZCO0.8 nanocrystalline film to conduct XPS analysis aiming at N 1s area. The peak at 400 eV often corresponds to C-N complex or N-N bond.⁶⁸ The possibility of C-N bond can be ruled out based on a C 1s scan result (Fig. S8). The N 1s peak at 400 eV in our samples is hence attributed to N atomic cluster formed in the process of ligand decomposition. An amazing peak featuring N_O species can be found at around 396.2 eV, clearly supportive of the formation of Zn-N bond.⁷ An evident chemical shift towards high binding energy direction, which is closer to Cu-N bond in CuN_3 (397.5 eV), indicates partial replacement of Zn-N by Cu-N. In spite of diffusion, uniform and smooth surface topology in Fig. 8f clearly shows the whole stability of dopant environment without observable aggregation.

Amine molecules can stabilize the structure of Cu related defects in terms of $\text{Cu-N}_{\text{amine}}$ bonds. Beyond that, we should emphasize the other role of ligand capping. Cu doped ZnO is a $\text{L}_{\text{VB}}\text{M}^{2+}\text{CT}$ -type system because $\text{Cu}^{2+} + E^* \rightarrow \text{Cu}^+ + h\nu_{\text{VB}} (E^* = h\nu + E_{\text{ion}})$, where E^* is total energy to finish CT, $h\nu \geq 2.859$ eV,⁶⁹ and E_{ion} is the ionization energy of $(\text{Cu}^+, h\nu_{\text{B}}) = 0.43$ eV from our previous work.² Hence, E^* is estimated to be *ca.* 3.289 eV. According to a localized charge-transfer model of Cu^{2+} in ZnO, the energy-level position of neutral Cu_{Zn} acceptor $[E(\text{Cu}^{2+})]$ is determined to lay 0.15 eV below the CBM, *i.e.* $E(\text{Cu}^{2+}) = E_{\text{g}}(3.44 \text{ eV}) - E(\text{Cu}^+) - E_{\text{ZPL}} = 0.15$ eV, where $E_{\text{ZPL}} = 2.860$ eV (ZPL denotes zero-phonon line) and $E(\text{Cu}^+)$ is the position of excited Cu_{Zn} state (0.43 eV mentioned above). Thus, an energy separation of 0.72 eV (0.87 eV-0.15 eV) between V_O and Cu acceptor could be calculated. This value is far higher than Xu *et al.* reported 149 meV about ferromagnetic ZnO:Cu nanowires.⁶⁹ Authors suggested that the small energy-level separation or exchange energy is prerequisite for dopant-defect hybridization. Therefore, the exchange interaction between V_O and Cu is not favorable in energy for amine-activated films and another consideration on *p-d* exchange mechanism, *i.e.* the hybridization between *d*-state and acceptor holes, should be taken.

Based on a delicate control of dopant concentration under low doping levels (0.2%, 0.5%, 0.8%, 1.0%, 1.2%, 1.5%), a decreased M_s trend can be clearly observed in Fig. 9c. These data demonstrate that the ferromagnetic ordering is indeed associated with Cu dopant. Even though grain boundary defects can partially mediate spin alignment, the increased magnitude in moment is still low unless amine ligands participate in this process (Fig. S11). Actually, this situation will not remain unchanged and increasing Cu concentration above 0.2% will reduce M_s due to the increased anti-ferromagnetic contribution.⁷⁰ Hence, the maximal effective net moment of 1.58 μ_{B}/Cu can be obtained in ZCO0.2 granular film. Since most thermally-activated films composed of OA-capped NCs display clear hysteresis loops (see Fig. 9a), some detailed characterizations should be conducted to confirm whether they are intrinsic or not. We first monitor the change of V_O^+ . It is noted that aggregated ZnO NCs (without OA capping) have less V_O^+ defect than free-standing ones in dispersions (see Fig. S12), which means V_O^+ defects are largely passivated in granular films. According to "Uncertainty Principle", the narrowed peak-to-peak line-width (ΔH_{pp}) of ESR signals should be ascribed to the increase of the electron-spin relaxation time and demonstrates a weak spin-coupling effect. Therefore, it can be inferred that interfacial fusion induced newly-formed grain boundary

defects would take away the electrons bound to V_O^+ and eventually lead to the decrease of ESR signal. In other words, the charge transfer from V_O^+ defects to Cu species is now replaced by the one from grain boundary defects to Cu species.

As earlier literature shown, grain boundary defects seem able to activate these paramagnetic Cu ions in NCs and exhibit ferromagnetic ordering.⁷¹ Even though the above opinion is reasonable, we only observe limited ferromagnetic enhancement without the aid of amine ligands (see Fig. S11). After OA molecules are linked to the surface of NCs, annealing induced Cu-N diffusion can not only enhance the magnitude of magnetization of ZnO:Cu but quench d^0 -ferromagnetism of ZnO (see Fig. S13). Kittilstved and Gamelin also found no room-temperature ferromagnetism for amine-capped ZnO nanoparticles.⁴ Even though their experimental result supported our case, a tiny difference still occurred in other reports.⁹ Actually, these differences from preparation method easily lead to the contradictory magnetic results, especially for surface capping perturbation.

Since the involvement of amine molecules will bring some considerations about the role of film texture, grain size and amorphous layers surrounding grains on ferromagnetic behavior,²¹ we next discuss these factors point to point. First, amine capping cannot affect the growth orientation of films and main diffraction peaks are basically unchanged (details see Fig. S14). The same annealing way in air would also not induce other possibilities and thus textures' effect can be excluded. Second, compared with a pair of AFM images from 0.2% doped film sample with and without amine capping in Fig. S15, tiny grain-size difference (20 nm and 18 nm) appears not to induce a huge magnetic variation. At last, we compared a pair of HRTEM images. As depicted in Fig. S16, the annealed film without amine capping exhibits a typical polycrystalline feature. Clear grain boundaries penetrate into all the grains and no observable amorphous layers are seen. On the contrary, amine-capped annealed granular film was coated by a dense amorphous area. Straumal *et al.*²¹ have experimentally revealed the role of this layer and its presence is adverse for enhancing saturation magnetization, especially for doped nanocrystalline film. We hereby deduce the above three factors do not play crucial effects on ferromagnetic ordering.

As our scenario, amine plays an acceptor-like role.⁴ On one hand, delocalized holes from N_O acceptors can hybrid with *d*-state of Cu ions. On the other hand, these acceptor defects can also compensate residual d^0 -ferromagnetism and this will be beneficial for Cu doping induced ferromagnetic ordering. Previous studies of ZnO:N revealed that the N_O acceptor energy-level was in the range of 170~200 meV.⁷² A minimal energy separation between $(\text{Cu}^+, h\nu_{\text{B}})$ state and N_O acceptor state is estimated to be 0.23 eV = 0.43 eV - 0.2 eV. This value is compatible with 0.22 eV for ferromagnetic *p*-type ZnO:Mn,⁷³ showing an ideal *p-d* exchange energy ($N_\text{O}\beta$). Besides N_O defect mediated *p-d* hybridization, how can we understand this kind of magnetic exchange interaction in other ways? For the possibility of charge-transfer ferromagnetism, according to Coey's theory,⁷⁴ its moment cannot exceed 1 μ_{B}/Cu . Actually, the moment value reported here is higher than 1 μ_{B}/Cu , which is beyond the scope of charge-transfer ferromagnetism mechanism. Spin-orbit coupling interaction can induce magnetization enhancement. Although the discrepancy of ionic size between Cu^+ and Cu^{2+} exists, a larger Cu^{2+} population than Cu^+ in the current case can only lead to the formation of less orbital states.⁷⁵ Thus, the contribution of spin-orbit coupling interaction should be not dominant. As for lattice polarization mechanism,⁷⁶ an inverse ferromagnetic dependence on dopant concentration can phenomenally meet our case. We have

known that, if doping concentration is 0.2%, the average distance between Cu ions in ZnO is about 35 nm. Such a long distance between magnetic ions at a high moment value implies a magnetic percolation mechanism involving the overlap of the regions of lattice polarization near magnetic ions, *i.e.* BMP (bound magnetic polaron) mechanism.⁷⁷ Hence, it is concluded that the formation of N_O acceptor defects not only contributes to the *p-d* hybridization but also the lattice polarization. But in any case, the origin of ferromagnetism is ultimately linked with N_O acceptor mediated magnetic exchange interaction.

Taken together, this kind of long-range exchange interaction is mainly realized by altering Cu-N electronic structure in ZnO, *i.e.* *p-d* hybridization of energy-band as described by perturbation theory. It is possible to easily fit *M-H* data by the following Langevin function.

$$M(H) = M_s \left(\frac{N^* H}{k_B T} - \frac{k_B T}{N^* H} \right) \quad (6)$$

Where M_s , k_B are constants, T is the temperature (300 K), H is the applied magnetic field, and N^* is the total magnetic moment of correlated paramagnetic unit (magnetic domain) within the film. Best fit to ZCO0.2 data yields an effective spin state of *ca.* 11600 Cu ions. In spite of inaccuracy of obtained data, but it provides an estimate for the dopant number involved in the ferromagnetic domain. For individual ZCO0.2 NC, it has on average only *ca.* 50 Cu ions per particle. This comparison suggests the participation of 200 or more NCs in a single ferromagnetic domain. Therefore, a type of strong hybridization mechanism with participation of N-capping should be responsible for the observed ferromagnetic ordering. In short, OA ligands containing N element can effectively link with every particle. Their presence not only overcomes grain boundary defects induced *d⁰*-ferromagnetism but couples with rarely-distributed Cu spin. More importantly, this strong exchange interaction is not able to live without Cu incorporation so the ferromagnetism in amine-activated ZnO:Cu granular film is intrinsic. Clearer experimental evidence of long-range ferromagnetic ordering by means of MFM has been given in Fig. 10. Except for a visible stripe-like magnetic domain structure, the high dependence on dopant concentration also confirms its intrinsic ferromagnetic genuine in our amine-activated ZnO:Cu system.

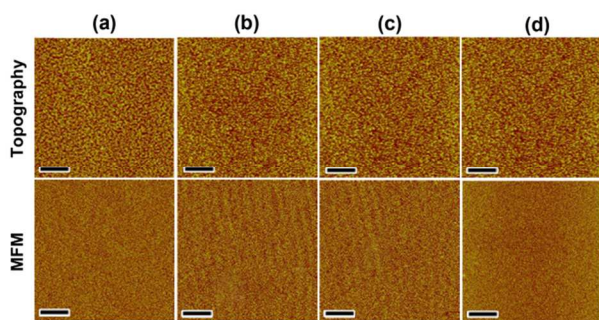


Fig. 10 A series of AFM topography and corresponding MFM images recorded from amine-activated (a) ZnO, (b) ZCO0.2, (c) ZCO1.0, and (d) ZCO2.0 granular films. The scale bar represents 5 μm .

3.5 Magnetic control strategy based donor and acceptor defects

Combined with our previous investigations,^{12, 17, 75} up to date, there have been three ways to control the ferromagnetism in ZnO:Cu film. One is tuning bulk defect composition (involving or vanishing those pivotal defect species), second is tuning surface defect polarity (N-capping or O-capping), and the last one is tuning charge transfer process *via* extrinsic physical perturbation (*e.g.* light). In order to realize highly efficient control, our hypothesis is that there must be appropriate

amounts of donor or acceptor defects in the bulk or surface of doped films.

In this report, we detailed discussed the role of N_O acceptor defect. For donor-like O-capping, we also took some attempts but the result was not ideal. TOPO (triocetylphosphine oxide) capping induced n-type surface perturbation cannot bring any magnetic response. As to this issue, we also did control experiments based on the variation of n-type defect density in the bulk rather than the surface.¹⁷ A strong dependence of magnetic ordering on donor concentration undoubtedly demonstrates the positive contribution of donor defect. But in fact there are limits on donor density. Excessive concentration will quench the ferromagnetism. These facts confirm a reliable donor-defect-mediated ferromagnetic origin and in practice the participated donor density cannot be too high, otherwise they will disturb spin alignment. Moreover, the perturbation of surface donor seems less effective than bulk donor, constituting a distinct donor-defect-mediated ferromagnetic activation scenario.

Actually, the diluted distribution of donor defects (V_O and Zn_i) can mediate long-range ferromagnetic ordering.² The corresponding indirect double exchange mechanism is highly-efficient (81.5% spin alignment). But for amine-activated films, a better saturation moment value (1.58 μ_B/Cu) than dual-donor magnetic exchange model (1.41 μ_B/Cu) was achieved. So which one should be more expected? In order to distinguish their difference between acceptor- and donor-defect-mediated ferromagnetic behaviour, we also list a series of *M-H* loops (Fig. 9b) from 900°C equilibrium thermal annealed film samples. In Fig. 9c, a maximal value occurs in 1.0% doped samples. At the entire doping content range, there is a first increased and then decreased trend, which can be explained by the competition between Cu spin state distribution and donor impurity band formation. For lightly-doped samples, due to inefficient coupling with donor impurity band, diluted Cu spins lead to a weak ferromagnetic response. But for the highly-concentrated involvement of Cu dopants, this case makes anti-ferromagnetic alignment of Cu spins possible. Therefore, a suitable donor defect density and Cu dopant distribution together define an optimum magnetic scenario (1.41 μ_B/Cu) in ZCO1.0 grain-coarsed film. In contrast, under acceptor polarization environment, 0.2% Cu doping has induced full *p-d* hybridization, implying the acceptor defect participated exchange process is more efficient than the donor defect participated one.

In Fig. 9d, acceptor and donor defect mediated ferromagnetic films both exhibit a clear bifurcation in ZFC/FC curves, confirming the nature of robust ferromagnetism. An effective utilization of magnetic moments in acceptor-defect-mediated ferromagnetic films can be deduced as 91.3%, accounting for the source of such a high moment value. The difference of moment between FC and ZFC curve, plotted in the inset of Fig. 9d as a function of temperature, clearly shows a different nature of magnetism in the amine-activated ferromagnetic samples, as indicated by the anomaly near 117 K. First, this temperature is not T_B , the blocking temperature, because for $T > T_B$, no hysteresis should be present, whereas in our case, hysteresis is observed up to 400 K. Second, Neel temperature (T_N) is sensitive to uncompensated Cu spins.^{23, 78} For Neel temperature (T_N) near 117 K, it suggests that some of the Cu spins are in the anti-ferromagnetic states. This is an important signature, fairly consistent with our previous analyses. Spin perturbation between the anti-ferromagnetically uncompensated spins and amine-activated spins extends T_c to

well above 400 K. Since amine activation efficiency is high enough, this scenario will serve the aim of controlling defect ferromagnetism by diverse means and reveals some novel physical processes. Along with dual-donor defect ferromagnetic model, the meaning of this work has two aspects: firstly, expand the opportunity of applications which utilize physical or chemical manipulation, and secondly, clarify the knowledge of using spin and defect (surface or bulk defects) as controllable states for the future spin-manipulation era. Subsequent investigations will be mainly focused on the subjects of defect engineering modulation and structural stability.

4 Summary and conclusions

Doping content tunable ZnO:Cu NCs were chemically derived through a nonequilibrium colloidal preparation technique. The energy-favourable combination between V_O defect and Cu species makes it possible to largely involve dopants into ZnO NC-based system, which is abided by trapped-dopant model. Metastable Cu dopants are pinned in VZISS located on the NCs' surface, where they are drastically reduced into neutral and monovalent state in terms of atomic-level planar clusters. Through two-pot amine processing, the coordination environment of Cu dopants changes a lot from interstitial sites to substitutional sites, accompanying with valence state variation. A bowed bandgap modification and enhanced Zn-O covalence feature verifies the occurrence of Cu-N bond diffusion. For such a process, there are several complex spatial configurations and valence state transformations. We simultaneously follow every evolution stage based on detailed analyses via a set of joint characterization techniques, e.g. XRD, EELS, XPS, UV-vis, IR, ESR, PL, etc. Such a combined methodology can be readily applied to other doped oxides.

Followed by a full discussion, we propose an N-acceptor related ferromagnetic activation route and compare the difference with donor-defect-mediated magnetic exchange process. Through amine annealing induced acceptor-like defects, these substitutional Cu spins can contribute to a maximal moment of $1.58 \mu_B/\text{Cu}$ in amine-capped 0.2% Cu-doped ZnO nanocrystalline films. The highest utilization of magnetic moment is up to 91.3%, better than dual-donor mediated ferromagnetic ordering (81.5%), indicating acceptor defect anticipated exchange process is more efficient than donor defect anticipated one. Their distinct spin-exchange process greatly inspires the development of defect ferromagnetic related mechanism and enriches the methodology of manipulating ferromagnetic "on/off" state. Besides, the particularity of Cu doping in ZnO still makes itself possess more advantages than other systems, such as simple bi-valence (Cu^+ and Cu^{2+}) control strategy and photo-sensitive defect behaviour, which will better serve some special fields.

Acknowledgements

This work was supported by National Natural Science Foundation of China 51372224, Program for Innovative Research Team in University of Ministry of Education of China (IRT13037), and National Science and Technology Support Program (2012BAC08B08)

Notes and references

State Key Laboratory of Silicon Materials, Department of Materials Science and Engineering, Zhejiang University, Hangzhou 310027, P. R. China.

Cyrus Tang Center for Sensor Materials and Applications, Zhejiang University, Hangzhou 310027, P. R. China

E-mail: zlp1@zju.edu.cn, hphe@zju.edu.cn; Fax: +86-571-87952625; Tel: +86-571-87951958

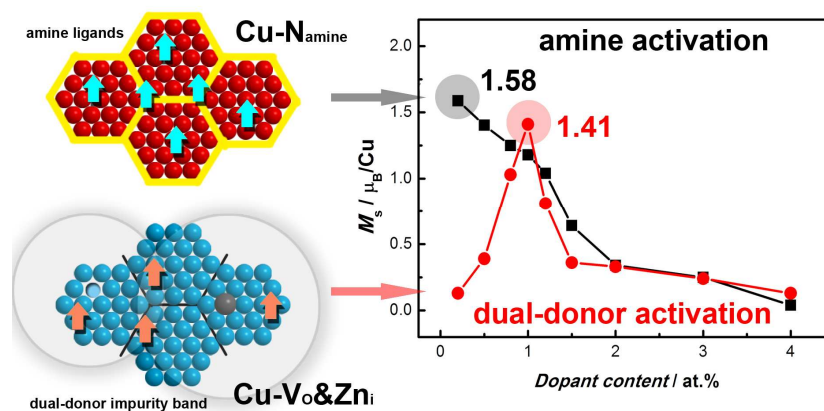
† Electronic Supplementary Information (ESI) available: Review table, XRD refined profiles, STEM and EDX results, morphology and topology photos of NCs and films, valence state analysis of Cu species, FT-IR and XPS related bonding analysis, some ESR and magnetic data for comparison. See DOI: 10.1039/b000000x/

1. D. Mocatta, G. Cohen, J. Schattner, O. Millo, E. Rabani and U. Banin, *Science*, 2011, **332**, 77-81; D. A. Schwartz, N. S. Norberg, Q. P. Nguyen, J. M. Parker and D. R. Gamelin, *J. Am. Chem. Soc.*, 2003, **125**, 13205-13218; T. Dietl, H. Ohno, F. Matsukura, J. Cibert and D. Ferrand, *Science*, 2000, **287**, 1019-1022; D. Wang, Q. Chen, G. Xing, J. Yi, S. R. Bakaul, J. Ding, J. Wang and T. Wu, *Nano Lett.*, 2012, **12**, 3994-4000.
2. L. Hu, J. Huang, H. He, L. Zhu, S. Liu, Y. Jin, L. Sun and Z. Ye, *Nanoscale*, 2013, **5**, 3918-3930.
3. Q. Ma, J. T. Prater, C. Sudakar, R. A. Rosenberg and J. Narayan, *J. Phys.: Condens. Matter*, 2012, **24**, 306002.
4. K. R. Kittilstved and D. R. Gamelin, *J. Am. Chem. Soc.*, 2005, **127**, 5292-5293.
5. D. J. Norris, A. L. Efros and S. C. Erwin, *Science*, 2008, **319**, 1776-1779.
6. M.-H. Du, S. C. Erwin and A. L. Efros, *Nano Lett.*, 2008, **8**, 2878-2882.
7. Y. Cheng, W. Hao, H. Xu, Y. Yu, T. Wang, R. Chen, L. Zhang, Y. Du, X. L. Wang and S. X. Dou, *ACS Appl. Mater. Interf.*, 2012, **4**, 4470-4475.
8. K. Kittilstved, N. Norberg and D. Gamelin, *Phys. Rev. Lett.*, 2005, **94**, 147209.
9. M. A. Garcia, J. M. Merino, E. F. Pinel, A. Quesada, J. de la Venta, M. L. R. Gonzalez, G. R. Castro, P. Crespo, J. Llopis, J. M. Gonzalez-Calbet and A. Hernando, *Nano Lett.*, 2007, **7**, 1489-1494.
10. C. Sudakar, J. S. Thakur, G. Lawes, R. Naik and V. M. Naik, *Phys. Rev. B*, 2007, **75**, 054423.
11. R. Beaulac, L. Schneider, P. I. Archer, G. Bacher and D. R. Gamelin, *Science*, 2009, **325**, 973-976; S. T. Ochsenein, Y. Feng, K. M. Whitaker, E. Badaeva, W. K. Liu, X. Li and D. R. Gamelin, *Nature Nanotech.*, 2009, **4**, 681-687.
12. L. Hu, L. Zhu, H. He, Y. Guo, G. Pan, J. Jiang, Y. Jin, L. Sun and Z. Ye, *Nanoscale*, 2013, **5**, 9577-9581.
13. S. T. Bromley, S. A. French, A. A. Sokol, C. R. A. Catlow and P. Sherwood, *J. Phys. Chem. B*, 2003, **107**, 7045-7057.
14. G. Z. Xing, J. B. Yi, J. G. Tao, T. Liu, L. M. Wong, Z. Zhang, G. P. Li, S. J. Wang, J. Ding, T. C. Sum, C. H. A. Huan and T. Wu, *Adv. Mater.*, 2008, **20**, 3521-3527; S. Yilmaz, E. McGlynn, E. Bacaksiz, S. Özcan, D. Byrne, M. O. Henry and R. K. Chellappan, *J. Appl. Phys.*, 2012, **111**, 013903; D. L. Hou, X. J. Ye, H. J. Meng, H. J. Zhou, X. L. Li, C. M. Zhen and G. D. Tang, *Appl. Phys. Lett.*, 2007, **90**, 142502.
15. A. Tiwari, M. Snure, D. Kumar and J. T. Abiade, *Appl. Phys. Lett.*, 2008, **92**, 062509.
16. T. S. Herng, D. C. Qi, T. Berlijn, J. B. Yi, K. S. Yang, Y. Dai, Y. P. Feng, I. Santoso, C. Sanchez-Hanke, X. Y. Gao, A. T. S. Wee, W. Ku, J. Ding and A. Rusydi, *Phys. Rev. Lett.*, 2010, **105**, 207201.
17. L. Hu, L. P. Zhu, H. P. He and Z. Z. Ye, *Appl. Phys. Lett.*, 2014, **104**, 062405.

- 18.S. Ogale, D. Kundaliya, S. Mehraeen, L.-f. Fu, S. Zhang, A. Lussier, J. Dvorak, N. Browning, Y. Idzerda and T. Venkatesan, *Chem. Mater.*, 2008, **20**, 1344-1352.
- 19.S. S. Farvid, N. Dave, T. Wang and P. V. Radovanovic, *J. Phys. Chem. C*, 2009, **113**, 15928-15933.
- 20.M. S. Park and B. I. Min, *Phys. Rev. B*, 2003, **68**, 224436.
- 21.B. B. Straumal, S. G. Protasova, A. A. Mazilkin, G. Schutz, E. Goering, B. Baretzky and P. B. Straumal, *JETP Lett.*, 2013, **97**, 367-377.
- 22.W. M. H. Oo, M. D. McCluskey, J. Huso, J. L. Morrison, L. Bergman, M. H. Engelhard and L. V. Saraf, *J. Appl. Phys.*, 2010, **108**, 064301.
- 23.X. Wang, J. B. Xu, W. Y. Cheung, J. An and N. Ke, *Appl. Phys. Lett.*, 2007, **90**, 212502.
- 24.X. Wang, J. B. Xu, N. Ke, J. Yu, J. Wang, Q. Li, H. C. Ong and R. Zhang, *Appl. Phys. Lett.*, 2006, **88**, 223108.
- 25.D. H. Xu and W. Z. Shen, *J. Phys. Chem. C*, 2012, **116**, 13368-13373; F. Ahmed, S. Kumar, N. Arshi, M. S. Anwar, S. Heo, G. Kim, J. Lu and B. Koo, *J. Korean Phys. Soc.*, 2012, **60**, 1644-1648.
- 26.J. Yoshihara, J. M. Campbell and C. T. Campbell, *Surf. Sci.*, 1998, **406**, 235-245.
- 27.S. A. French, A. A. Sokol, C. R. A. Catlow and P. Sherwood, *J. Phys. Chem. C*, 2008, **112**, 7420-7430.
- 28.Z. Zhang, J. B. Yi, J. Ding, L. M. Wong, H. L. Seng, S. J. Wang, J. G. Tao, G. P. Li, G. Z. Xing, T. C. Sum, C. H. Alfred Huan and T. Wu, *J. Phys. Chem. C*, 2008, **112**, 9579-9585.
- 29.R. D. Leapman, L. A. Grunes and P. L. Fejes, *Phys. Rev. B*, 1982, **26**, 614-635.
- 30.Y. Cheng, W. Hao, H. Xu, Y. Yu, T. Wang, R. Chen, L. Zhang, Y. Du, X. L. Wang and S. X. Dou, *ACS Appl. Mater. Interf.*, 2012, **4**, 4470-4475; Y. Cheng, R. Chen, H. Feng, W. Hao, H. Xu, Y. Wang and J. Li, *Phys. Chem. Chem. Phys.*, 2014, **16**, 4544-4550.
- 31.M. Ferhat, A. Zaoui and R. Ahuja, *Appl. Phys. Lett.*, 2009, **94**, 142502.
- 32.R. W. Martin, P. G. Middleton, K. P. O'Donnell and W. Van der Stricht, *Appl. Phys. Lett.*, 1999, **74**, 263-265.
- 33.N. S. Pesika, K. J. Stebe and P. C. Searson, *Adv. Mater.*, 2003, **15**, 1289-1291.
- 34.R. B. Bylisma, W. M. Becker, J. Kossut, U. Debska and D. Yoder-Short, *Phys. Rev. B*, 1986, **33**, 8207-8215.
- 35.R. Viswanatha, S. Chakraborty, S. Basu and D. D. Sarma, *J. Phys. Chem. B*, 2006, **110**, 22310-22312; R. Viswanatha, S. Sapra, S. Sen Gupta, B. Satpati, P. V. Satyam, B. N. Dev and D. D. Sarma, *J. Phys. Chem. B*, 2004, **108**, 6303-6310.
- 36.Q. Ma, D. B. Buchholz and R. P. H. Chang, *Phys. Rev. B*, 2008, **78**, 214429.
- 37.G. Clavel, M.-G. Willinger, D. Zitoun and N. Pinna, *Adv. Funct. Mater.*, 2007, **17**, 3159-3169.
- 38.B. Balamurugan and B. R. Mehta, *Thin Solid Films*, 2001, **396**, 90-96.
- 39.K. X. Yao, X. M. Yin, T. H. Wang and H. C. Zeng, *J. Am. Chem. Soc.*, 2010, **132**, 6131-6144.
- 40.M. Nakayama, M. Kaneko, Y. Uchimoto, M. Wakihara and K. Kawamura, *J. Phys. Chem. B*, 2004, **108**, 3754-3759.
- 41.H.-M. Xiong, D. G. Shchukin, H. Moehwald, Y. Xu and Y.-Y. Xia, *Angew. Chem. Int. Edit.*, 2009, **48**, 2727-2731.
- 42.S. C. Erwin, L. J. Zu, M. I. Haftel, A. L. Efros, T. A. Kennedy and D. J. Norris, *Nature*, 2005, **436**, 91-94.
- 43.P. Lommens, F. Loncke, P. F. Smet, F. Callens, D. Poelman, H. Vrielinck and Z. Hens, *Chem. Mater.*, 2007, **19**, 5576-5583.
- 44.P. V. Radovanovic and D. R. Gamelin, *J. Am. Chem. Soc.*, 2001, **123**, 12207-12214.
- 45.A. V. Isarov and J. Chrysochoos, *Langmuir*, 1997, **13**, 3142-3149.
- 46.S. B. Zhang, S. H. Wei and A. Zunger, *Phys. Rev. B*, 2001, **63**, 075205.
- 47.A. L. Roest, J. J. Kelly, D. Vanmaekelbergh and E. A. Meulenkamp, *Phys. Rev. Lett.*, 2002, **89**, 036801.
- 48.R. Viswanatha, P. K. Santra, C. Dasgupta and D. D. Sarma, *Phys. Rev. Lett.*, 2007, **98**, 255501.
- 49.A. Punnoose, M. S. Seehra, B. C. Dunn and E. M. Eyring, *Energ. Fuel*, 2002, **16**, 182-188.
- 50.G. Leofanti, M. Padovan, M. Garilli, D. Carmello, A. Zecchina, G. Spoto, S. Bordiga, G. T. Palomino and C. Lamberti, *J. Catal.*, 2000, **189**, 91-104.
- 51.A. Baiker, D. Monti and A. Wokaun, *Appl. Catal.*, 1986, **23**, 425-436.
- 52.A. Janotti and C. G. Van de Walle, *Phys. Rev. B*, 2007, **76**, 165202.
- 53.F. Gallino and C. Di Valentin, *J. Chem. Phys.*, 2011, **134**, 144506.
- 54.A. Hausmann, B. Schallenger and R. Roll, *Zeitschrift Fur Physik B: Condens. Matter*, 1980, **40**, 1-7.
- 55.C. Sigwart, Hemmeric.P and J. T. Spence, *Inorg. Chem.*, 1968, **7**, 2545-2548.
- 56.H. So, *Bull. Korean Chem. Soc.*, 1987, **8**, 111.
- 57.T. S. Herng, S. P. Lau, S. F. Yu, H. Y. Yang, K. S. Teng and J. S. Chen, *J. Phys.: Condens. Matter*, 2007, **19**, 356214.
- 58.G. H. Kim, D. L. Kim, B. D. Ahn, S. Y. Lee and H. J. Kim, *Microelectr. J.*, 2009, **40**, 272-275; P. Fons, A. Yamada, K. Iwata, K. Matsubara, S. Niki, K. Nakahara and H. Takasu, *Nuclear Instruments & Methods in Physics Research Section B-Beam Interactions with Materials and Atoms*, 2003, **199**, 190-194.
- 59.R. E. Dietz, H. Kamimura, A. Yariv and M. D. Sturge, *Phys. Rev.*, 1963, **132**, 1559-1569.
- 60.R. Dingle, *Phys. Rev. Lett.*, 1969, **23**, 579-581.
- 61.P. Dahan and V. Fleurov, *Phys. Rev. B*, 1996, **53**, 12845-12854.
- 62.L. Zhang, L. Yin, C. Wang, N. Lun, Y. Qi and D. Xiang, *J. Phys. Chem. C*, 2010, **114**, 9651-9658.
- 63.P. V. Kamat and B. Patrick, *J. Phys. Chem.*, 1992, **96**, 6829-6834.
- 64.N. S. Norberg and D. R. Gamelin, *J. Phys. Chem. B*, 2005, **109**, 20810-20816.
- 65.G. Xing, G. Xing, M. Li, E. J. Sie, D. Wang, A. Sulistio, Q.-L. Ye, C. H. A. Huan, T. Wu and T. C. Sum, *Appl. Phys. Lett.*, 2011, **98**, 102105.
- 66.N. Garces, L. Wang, L. Bai, N. Giles, L. Halliburton and G. Cantwell, *Appl. Phys. Lett.*, 2002, **81**, 622-624.
- 67.D. B. Buchholz, R. P. H. Chang, J. H. Song and J. B. Ketterson, *Appl. Phys. Lett.*, 2005, **87**, 082504; G.-P. Qin, X.-Q. Wang, J. Zheng, C.-Y. Kong, H.-B. Ruan, W.-J. Li, Y.-H. Zhao and X.-D. Meng, *Chinese Phys. B*, 2013, **22**, 057101; P. Liang and X. Ma, *J. Synth. Cryst.*, 2010, **39**, 1067-1071.
- 68.C. L. Perkins, S. H. Lee, X. N. Li, S. E. Asher and T. J. Coutts, *J. Appl. Phys.*, 2005, **97**, 034907; M. Petravic, P. N. K. Deenapanray, V. A. Coleman, C. Jagadish, K. J. Kim, B. Kim, K. Koike, S. Sasa, M. Inoue and M. Yano, *Surf. Sci.*, 2006, **600**, L81-L85; L. Sun, H. He, L. Hu and Z. Ye, *Phys. Chem. Chem. Phys.*, 2013, **15**, 1369-1373.

- 69.H. J. Xu, H. C. Zhu, X. D. Shan, Y. X. Liu, J. Y. Gao, X. Z. Zhang, J. M. Zhang, P. W. Wang, Y. M. Hou and D. P. Yu, *J. Phys.: Condens. Matter*, 2010, **22**, 016002.
- 70.Y. F. Tian, Y. F. Li, M. He, I. A. Putra, H. Y. Peng, B. Yao, S. A. Cheong and T. Wu, *Appl. Phys. Lett.*, 2011, **98**, 162503.
- 71.P. I. Archer, P. V. Radovanovic, S. M. Heald and D. R. Gamelin, *J. Am. Chem. Soc.*, 2005, **127**, 14479-14487; J. D. Bryan, S. A. Santangelo, S. C. Keveren and D. R. Gamelin, *J. Am. Chem. Soc.*, 2005, **127**, 15568-15574.
- 72.D. C. Look and B. Claftin, *Physica Status Solidi B-Basic Solid State Physics*, 2004, **241**, 624-630; D. C. Look, D. C. Reynolds, C. W. Litton, R. L. Jones, D. B. Eason and G. Cantwell, *Appl. Phys. Lett.*, 2002, **81**, 1830-1832.
- 73.K. R. Kittilstved, W. K. Liu and D. R. Gamelin, *Nat. Mater.*, 2006, **5**, 291-297.
- 74.J. M. D. Coey, K. Wongsaprom, J. Alaria and M. Venkatesan, *J. Phys. D. Appl. Phys.*, 2008, **41**, 134012.
- 75.L. Hu, L. Zhu, H. He and Z. Ye, *Appl. Phys. Lett.*, 2014, **105**, 072414.
- 76.A. F. Orlov, N. S. Perov, L. A. Balagurov, A. S. Konstantinova and D. G. Yarkin, *JETP Lett.*, 2007, **86**, 352-354.
- 77.J. M. D. Coey, M. Venkatesan and C. B. Fitzgerald, *Nat. Mater.*, 2005, **4**, 173-179.
- 78.A. Punnoose, H. Magnone, M. S. Seehra and J. Bonevich, *Phys. Rev. B*, 2001, **64**, 174420.

TOC Figure



Acceptor defect: a more efficient ferromagnetic activation route than donor defect in Zn-Cu-O dilute magnetic semiconductor